Hindawi
Journal of Electrical and Computer Engineering
Volume 2023, Article ID 9846375, 1 page
https://doi.org/10.1155/2023/9846375

Retraction

Retracted: Optimal Design of Vehicle Structure Based on Computer-Aided Technology

Journal of Electrical and Computer Engineering

Received 19 December 2023; Accepted 19 December 2023; Published 20 December 2023

This article has been retracted by Hindawi following an investigation undertaken by the publisher [1]. This investigation has uncovered evidence of one or more of the following indicators of systematic manipulation of the publication process:

(1) Discrepancies in scope

(2) Discrepancies in the description of the research reported

(3) Discrepancies between the availability of data and the research described

(4) Inappropriate citations

(5) Incoherent, meaningless and/or irrelevant content included in the article

(6) Manipulated or compromised peer review

The presence of these indicators undermines our confidence in the integrity of the article's content and we cannot, therefore, vouch for its reliability. Please note that this notice is intended solely to alert readers that the content of this article is unreliable. We have not investigated whether authors were aware of or involved in the systematic manipulation of the publication process.

Wiley and Hindawi regrets that the usual quality checks did not identify these issues before publication and have since put additional measures in place to safeguard research integrity.

We wish to credit our own Research Integrity and Research Publishing teams and anonymous and named external researchers and research integrity experts for contributing to this investigation.

The corresponding author, as the representative of all authors, has been given the opportunity to register their agreement or disagreement to this retraction. We have kept a record of any response received.

References

[1] G. Bai, "Optimal Design of Vehicle Structure Based on Computer-Aided Technology," *Journal of Electrical and Computer Engineering*, vol. 2022, Article ID 3326126, 9 pages, 2022.

Hindawi
Journal of Electrical and Computer Engineering
Volume 2022, Article ID 3326126, 9 pages
https://doi.org/10.1155/2022/3326126

Research Article

Optimal Design of Vehicle Structure Based on Computer-Aided Technology

Guang Bai

Baicheng Normal University, Baicheng, Jilin 137000, China

Correspondence should be addressed to Guang Bai; bg18343686898@163.com

Received 7 April 2022; Accepted 9 May 2022; Published 31 May 2022

Academic Editor: Wei Liu

In order to improve the optimization design effect of modern automobile vehicle structure, this paper combines computer-aided technology to carry out vehicle structure optimization design, introduces the material description of the collision process, expounds the boundary conditions in the collision process, and introduces the theory of explicit integration algorithm. In the simulation process, it is necessary to deal with time step control, contact algorithm, hourglass control, etc., and analyze the optimization method of automobile collision, which is divided into experimental design and optimization method. In addition, the experimental design mainly introduces the orthogonal experimental design, which is applied to the lightweight design of automobile structures. The research verifies that computer-aided technology can play an important role in vehicle structure optimization and effectively improve the scientificity of vehicle structure design.

1. Introduction

Structural optimization is widely used in machine design and has become a commonly used computer-aided engineering (CAE) tool in the automotive and aircraft industries. On the other hand, structural optimization methods have not been widely used in railway vehicle design, although there are some examples of railway vehicles using this optimization method. In order to achieve various purposes, such as better safety, higher speed, and better ride comfort, the body structure of railway vehicles needs to be improved. Crash safety design is one such need for increased safety, which tends to increase the mass of the vehicle body structure. Therefore, there is a need to find structures that are lighter in mass and more rigid. This is exactly where the structural optimization method can effectively support the design of the vehicle body structure. Previous studies on conventional plate girder car body structures using structural optimization methods to reduce mass and enhance strength have confirmed the effectiveness of structural optimization methods.

Compared with general mechanical parts and mechanism optimization, structural optimization is more difficult, because the objective function and constraint function of the latter can often be expressed as explicit functions of design variables. Structural optimization design must adopt unique and more effective optimization methods. Rational criterion method is a kind of effective method for structure optimization, including virtual work criterion method [1] and weight criterion method [2], which are popular at home and abroad, which are characterized by virtual work expression for displacement. The rational criterion method is to derive the criterion equations that the optimal structure must satisfy according to the Lagrangian condition of the equality-constrained optimization problem or the Kuhn–Tucker condition of the inequality-constrained optimization problem and gradually approach the optimum by solving the criterion equations iteratively. The rational criterion method has fast convergence and small computational workload, especially in the first few steps of optimization iteration; the optimization effect is obvious. The rational criterion method overcomes the shortcoming that the perceptual criterion method such as the full stress method is separated from the mathematical extreme value theory, and the rational criterion method for structural optimization design should be able to obtain the optimal solution of the original structural

optimization problem. Many people believe that the criterion method has shortcomings in the paper review [3]: (1) it is not rigorous and cannot find the optimal solution. (2) It is necessary to artificially distinguish between critical constraints and noncritical constraints. (3) The scope of application is narrow, etc. This is only the shortcoming of the early perceptual criterion method, which has been overcome by the guided weight method.

The research work of pedestrian protection is different from the development of occupant protection. When an accident occurs, due to the changeable states of pedestrians, the damage caused by different states is quite different, so the collision of pedestrians has great uncertainty [4]. Literature [5] and Literature [6] carried out statistical analysis of pedestrian traffic accident cases and based on this analyzed the causes and characteristics of pedestrian injuries in accidents, as well as the environmental characteristics of pedestrian accidents, including accident time, road condition, vehicle type, damage location, speed distribution, pedestrian age and gender distribution, and other basic information; people-vehicle collision accidents are classified. With the deepening of the work, the research on pedestrian protection has gradually shifted from the research on accident causes and damage mechanisms to the forward development of vehicle models [7]. Different reproduction methods are used to complete the collision experiment between pedestrians and vehicles. Through the study of accident laws in reproduction experiments, prediction and exploration of methods to prevent accidents and reduce economic losses have been fully recognized in the research work of pedestrian protection [8]. So far, the research methods of pedestrian protection mainly include real vehicle crash test of dummy model, real vehicle crash test of component impactor model, and mathematical analysis method, etc. [9].

The finite element method utilizes the idea of discreteness to disperse the elastic continuum hypothetically into a collection of finite elements. Through the analysis of each discrete element, an approximate solution that meets the accuracy requirements of the problem is obtained.

Literature [10] proposed a method to calculate the fatigue life of structural solder joints based on the frequency domain method, obtains the SN curve of the solder joint material through uniaxial tensile experiments, obtains the transfer function of the structural response combined with the vibration experiment, and inputs the PSD power spectrum of the vibration signal. The fatigue life of the solder joint is obtained from the density, and finally the correctness of the method is verified by experiments. Compared with the time domain method, the calculation speed of this method is faster, but the experimental cost is higher. Literature [11] took a certain type of light rail vehicle as an example and compares two different fatigue life methods. The difference between the two methods is that the load on the structure is considered as the horizontal load and the random load, and the notch of the structure is also considered. Finally, it is believed that considering the loads on the structure as random loads can get more realistic results. Literature [12] used an equivalent load method to calculate the fatigue life of the structure. This method can roughly predict the fatigue life of the structure, but it ignores the effect of random dynamic loads on the fatigue of the structure. Literature [13] used the structural vibration acceleration power spectrum data based on the CAE simulation platform to calculate the fatigue life of the structure from the perspective of the time domain, and it is verified by a case. This method is suitable for the situation with more vibration test data. Literature [14] took the EMU car body as the research object, used multi-body dynamics simulation combined with finite element analysis, and combined with the main S–N curve of the structure to predict the fatigue life of the weld in the local fatigue-prone region of the car body. Literature [15] analyzed the fatigue crack problem of K6 car seat. By combining simulation and experimental data, the fatigue area of the structure was obtained based on the nominal stress analysis method, and the structure was optimized according to the analysis results. Literature [16] took the monorail vehicle bogie frame as the research object, and based on the finite element analysis and calculation results, the fatigue life of the structure was predicted based on the nominal stress method, and the structural static strength and fatigue strength of the frame were checked. Literature [17] took the K6 bogie as an example and used the fatigue analysis algorithm of rigid-flexible coupling to predict the fatigue parts of the structure by means of dynamic stress recovery and combined the material S-N curve to predict the fatigue life of the structure. Literature [18] took the SW-220 K bogie frame as the research object, obtained the boundary load spectrum combined with the dynamic simulation, and obtained the stress distribution and fatigue life of the structure combined with the finite element analysis. Literature [19] selected several fatigue risk measurement points through the measured dynamic stress experiment for evaluation and used rainflow counting to compile the load spectrum to predict the fatigue life of the structure. This method is based on reality, but the dynamic stress experiment is relatively expensive and is greatly affected by the line, passenger capacity, and climate, so the dynamic stress experiment is only suitable for a certain type of vehicle in a certain line section and has no universality. Literature [20] established the finite element model of the frame according to the strength check standard and checked the static strength and fatigue strength of the frame. Since the actual frame is subjected to random dynamic loads, it is relatively more reasonable to apply dynamic loads to the frame for fatigue analysis. Literature [21] introduced the main S-N curve into the fatigue life prediction of welds in the early stage of structural design. This method can well identify the stress concentration of welds on complex structures and has guiding significance for structural design modifications. Literature [22] took a certain type of frame as an example and predicted the fatigue life of the structure based on the results of the structural strength analysis combined with the virtual fatigue simulation platform, but the dynamic load used in the fatigue analysis process is cyclic symmetrical dynamic load, and it is subjected to random dynamic loads, so the results that may be obtained by using random dynamic loads as the input of fatigue analysis are relatively more reasonable.

In this paper, the computer-aided technology is used to carry out the optimal design of the vehicle structure, and the effect of the method is verified through experimental research, which promotes the improvement of the effect of the computer-aided technology for the optimal design of the vehicle structure.

2. Computer-Aided Vehicle Structural Optimization

2.1. Finite Element Theory of Automobile Crash and Its Optimization Method. Vehicle crash is a nonlinear dynamic response process with large displacement and large deformation. The main methods to solve the collision problem are the finite element method and the multi-body system dynamics method. This section mainly introduces the finite element method. In the process of automobile collision, contact and high-speed impact are its core processes. For multiple nonlinear problems, the finite element method can discretize continuous space problems and decompose these complex nonlinear physical phenomena into elements connected by nodes, so as to obtain the force situation of the desired position in the collision, intrusion, speed, acceleration, and other physical quantities, and can also analyze the damage of the occupants in the car. The advantage of the finite element method is that the cost is low, the model can be reused, and the collision problem is combined with the computing power of the computer. This section will introduce the basic theory and optimization methods in the car crash problem.

From a physical point of view, the collision process is the process from the time $t = 0$ when the collision occurs to the time $t > 0$ when the collision ends. Researchers can analyze the various responses generated during this time period and can also perform transient analysis at a certain moment alone. The entire collision process must satisfy the following equations.

We assume that the position coordinate of the particle at the initial time is $X_i\,(i = 1, 2, 3)$, and after time t, the particle is transformed to a new position coordinate, the coordinate is $x_i\,(i = 1, 2, 3)$, and then the movement process of the particle from the initial time to time t can be expressed by the following formula:

$$x_i = x_i(X_i, t), \quad i = 1, 2, 3. \tag{1}$$

When $t = 0$, there are initial conditions:

$$\begin{aligned} x_i(X_i, 0) &= X_i, \quad i = 1, 2, 3, \\ \dot{x}_l(X_i, 0) &= v_i(X_i), \quad i = 1, 2, 3. \end{aligned} \tag{2}$$

In the formula, v_i represents the initial velocity of the particle, and the law of conservation of momentum must be satisfied for the interior of the object. From the Cauchy momentum equation, we get

$$\sigma_{ij,i} + \rho f_i = \rho \ddot{x}_l. \tag{3}$$

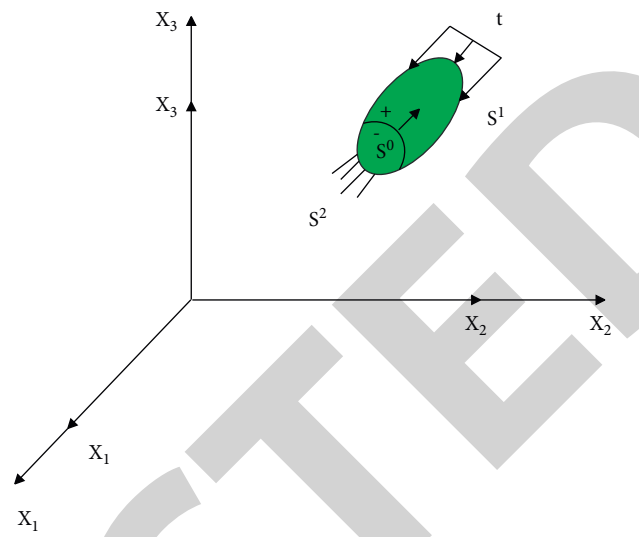

Figure 1: Sketch of the boundary conditions of the deformed object.

In the formula, $\ddot{x}_l$ is the acceleration, f_i is the body force per unit mass (body force density), and σ_{ij} is the Cauchy stress tensor. The relationship between ρ and ρ_0 is

$$\rho V = \rho_0. \tag{4}$$

In the formula, ρ is the instantaneous mass density, ρ_0 is the reference density, and V is the relative volume.

2.2. Boundary Conditions during Collision. There are three kinds of boundary conditions for deformed objects: surface force boundary conditions, displacement boundary conditions, and boundary conditions between two contact surfaces. The schematic diagram of the boundary conditions of the deformed object is shown in Figure 1.

For the surface force boundary condition, the surface force boundary condition on the S^1 surface satisfies

$$\sigma_{ij} n_j = t_i(t) \quad i, j = 1, 2, 3. \tag{5}$$

In the formula, σ_{ij} is the Cauchy stress tensor, n_j is the cosine in the direction of the outer normal on the S^1 surface, and t_i is the surface force load on the S^1 surface.

For the displacement boundary condition, the displacement boundary condition on the S^2-plane satisfies

$$x_i\left(X_j, t\right) = D_i(t) \quad i, j = 1, 2, 3. \tag{6}$$

In the formula, $D_i(t)$ is the given displacement function.

For the boundary conditions at the two contact surfaces, in Figure 1, the surface S^0 is the contact point between the surface S^1 and the surface S^2. When $x_i^+ = x_i^-$, the boundary condition of the surface S^0 satisfies

$$\left(\sigma_{ij}^+ - \sigma_{ij}^-\right) v_j = 0 \quad i, j = 1, 2, 3. \tag{7}$$

In the formula, σ_{ij} is the Cauchy stress tensor and v_j is the cosine in the direction of the outer normal on the face S^0.

Equation (7) is transformed into a variational formula whose integral equation simplification can eventually become the virtual work principle, which means that the sum of the virtual work of the external and internal forces on the object is zero.

2.3. Explicit Integration Algorithm. When establishing the finite element equation of deformable body, two methods are mostly used: one is the Euler description method for fluid mechanics, and the other is the Lagrange method for solid mechanics. In particular, for the typical transient nonlinear large deformation problem of automobile collision, the explicit integration algorithm is its typical calculation method. The nonlinear deformation body dynamics equation is shown as follows:

$$M\ddot{u}(t) + C\dot{u}(t) + Ku(t) = P(t). \tag{8}$$

In the formula, $\ddot{u}$ is the mass matrix, h is the nodal acceleration matrix, C is the damping matrix, $\dot{u}$ is the nodal velocity matrix, K is the stiffness matrix, and u is the nodal displacement matrix. P represents the received load vector matrix (the load vector matrix includes the total load of external forces, such as nodal load, surface force, body force, etc.).

The more commonly used method of solving (8) is the step-by-step integration method. The step-by-step integration method can be divided into Houbolt method, Wilson-θ method, Newmark method, and central difference method. As a complex nonlinear dynamic problem, the car collision problem is generally solved by the central difference method in order to ensure its convergence. This article uses the explicit central difference algorithm in the LS-DYNA software.

The solution time period is divided into $0, \ldots\ldots, t_n$. Under the premise that the solution of the time step of $0, \ldots\ldots, t_n$ is known, the kinematic equation of (8) can be changed into

$$M\ddot{u}(t_n) = P(t_n) - F_{\text{int}}(t_n) + H(t_n) - C\dot{u}(t_n). \tag{9}$$

In the formula, $F_{\text{int}}(t_n)$ represents the internal force vector, which includes the unit internal force and contact force, and $H(t_n)$ represents the hourglass resistance. When (9) puts the mass matrix to the right, the acceleration at time b can be obtained as

$$\ddot{u}(t_n) = M^{-1}[P(t_n) - F_{\text{int}}(t_n) + H(t_n) - C\dot{u}(t_n)]. \tag{10}$$

The velocity and displacement of the node can be obtained from the following:

$$\dot{u}\left(t_{n+(1/2)}\right) = \dot{u}\left(t_{n-(1/2)}\right) + \ddot{u}(t_n)\Delta t_n, \tag{11}$$

$$u(t_{n+1}) = u(t_n) + \dot{u}\left(t_{n+(1/2)}\right)\Delta t_{n+(1/2)}. \tag{12}$$

In (12), $\Delta t_{n+(1/2)} = \Delta t_n + \Delta t_{n+1}/2$.

From (12), the displacement of the node at time t_{n+1} can be obtained, and after the displacement is obtained, the geometric configuration of the system at the new time can be obtained. Because the mass matrix M is a lumped mass matrix, the motion process is not coupled, and the overall stiffness matrix does not need to be integrated in the solution process, which reduces the amount of data storage and improves the computational efficiency, thereby reducing the solution time.

2.4. Time Step Control for Explicit Integration Algorithms. Since the central difference method uses the mass matrix and the central single-point integral, an extended linear relationship is used for the changes of displacement and acceleration in the solution process. This requires that the time step should not be too large; otherwise the results may be distorted and the real response cannot be accurately expressed during the simulation calculation. If the time step size is too small, the calculation time will increase sharply, and the calculation process cannot even be completed. Therefore, choosing a reasonable time step is crucial to a successful simulation process. When the time step Δt is larger than the critical time step Δt_c, the solution process is extremely unstable; that is, the time step Δt must satisfy

$$\Delta t \le \Delta t_c = \frac{2}{\omega_{\max}}. \tag{13}$$

In the formula, $\omega_{\max}$ is the natural frequency of the highest order vibration of the system. The critical time step of an element is related not only to the characteristic length of the element, but also to the material properties. Therefore, the mesh quality must be controlled in the finite element analysis process to ensure the accuracy of the simulation process.

The following are the formulas for calculating the critical step size of several common units:

(1) The critical time step calculation of rod element and beam element is

$$\Delta t_c = \frac{L}{c}, \tag{14}$$

$$c = \sqrt{\frac{E}{\rho}}, \tag{15}$$

where L is the characteristic length of the beam element and the rod element, c is the wave speed of the material, E is the elastic modulus of the material, and ρ is the density of the material.

(2) The critical time step calculation for shell elements is

$$\Delta t_c = \frac{L_s}{c}, \qquad c = \sqrt{\frac{E}{\rho\left(1 - \nu^2\right)}}. \tag{16}$$

In the formula, L_s is the characteristic length of the shell element and v is the Poisson's ratio of the material. For triangular and quadrilateral shell

elements, the most common among shell elements, the characteristic length L_s can be derived from

$$\text{Triangular shell element}: L_S = \frac{2A}{\max(L_1, L_2, L_3)},$$
$$\text{Quadrilateral shell elements}: L_S = \frac{A}{\max(L_1, L_2, L_3, L_4)}. \quad (17)$$

In the formula, A is the area of the shell element, and $L_i\,(i = 1, 2, 3, 4)$ is the length of each side of the shell element.

(3) The critical step size calculation for solid elements is

$$\Delta t_c = \frac{L_s}{Q + \sqrt{Q^2 + c^2}}, \quad (18)$$
$$Q = \begin{cases} 0, & \varepsilon \geq 0, \\ C_1 c + C_0 L_s |\varepsilon|, & \varepsilon < 0. \end{cases}$$

In the formula, C_0 takes 0.06 and C_1 takes 1.5, both of which are constants.

For the more common 6-node solid elements and 8-node solid elements in solid elements, the characteristic length L_s can be derived from the following formula:

$$\text{6 node solid element}: L_s = \frac{3V}{A_{\text{mac}}},$$
$$\text{8 node solid element}: L_s = \frac{V}{A_{\text{mac}}}. \quad (19)$$

In the formula, V is the volume of the solid element, and A_{mac} is the largest lateral area of the solid element.

During finite element simulation, the smallest size element determines the time step for the model as a whole. If there are very few small-sized elements in the model, this will directly lead to increased computation time. In order to eliminate this phenomenon and control the calculation time, the technique of mass scaling can be used to adjust the time step without changing the finite element model.

Taking the shell element as an example, the time step setting is shown in Figure 2.

As shown in the figure, there are 3 shell elements; then,

$$\Delta t_{c\min} = \frac{l_{\min}}{c} = \frac{l_3}{c}, \quad (20)$$
$$c = \sqrt{\frac{E}{\rho(1 - \nu^2)}}.$$

From (14), it can be known that $\Delta t \leq \Delta t_{c\min}$. Therefore, in order to ensure the convergence of the calculation, it is necessary to make $\Delta t_{c\min}$ as large as possible, that is, to make c smaller. This can be achieved by increasing the elastic modulus E or reducing the material density ρ. Since the true elastic modulus value is required in the contact, it can only be achieved by adjusting the material density ρ, which is mass scaling.

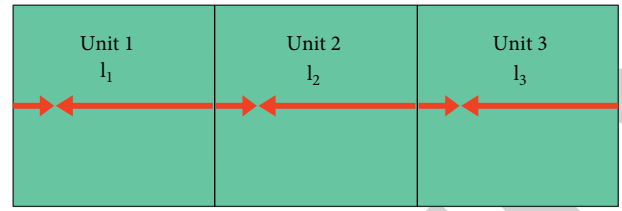

Figure 2: Sketch of a shell element.

Since mass scaling will change the mass and centroid position of the model, a large range of mass scaling will have a relatively large impact on the results, and a small range of mass scaling will not affect the results and greatly shorten the computation time. It is generally believed that the system quality control increased by mass scaling is optimal within 5%.

Specifically, in LS-DYNA, the quality scaling can be set through the TSSFAC and DT2MS tabs in the keyword ∗ CONTROL_TIMESTEP. When DT2MS is positive, it means mass scaling for all elements. When the DT2MS value is 0, it means no mass scaling. When DT2MS is negative, it means to scale the cells whose time step is less than |TSSFAC ∗ DT 2 MS|. This is the recommended quality scaling for a small range.

3. Experimental Research

This paper takes the car door as the research object to carry out the application of computer-aided technology in the optimization design of vehicle structure.

In order to effectively analyze the car door structure, it is necessary to carry out structural analysis on it, on the basis of meeting the performance requirements of the car body structure. To analyze the door structure, it needs to achieve a certain rigidity, and the door department needs to withstand tens of thousands of impacts, and its impact structure performance needs to be met in the process of structural optimization. The door structure diagram is shown in Figure 3.

The finite element analysis of the door structure is carried out. In Figure 2, A-E are used to represent the reinforcing plate, inner and outer plates, anticollision beams, brackets, and outer plate structures of the door. The outer plate structure mainly includes 8834 nodes and 9033 shell elements. The stress analysis shows that there are three main situations in its stiffness part, as shown in Figure 2: sag stiffness (F_{sag}), upper lateral stiffness (F_{upper}), and lower lateral stiffness (F_{lower}). The sag stiffness (F_{sag}) of the door is caused by the fact that the door is constrained by the hinge, resulting in a downward load when the door is locked out, and the load is concentrated at one point. The statistical results show that the load size is within [600 N, 1000 N], and the mean value is expressed as 800 N. The upper lateral stiffness (F_{upper}) and the lower lateral stiffness (F_{lower}) are

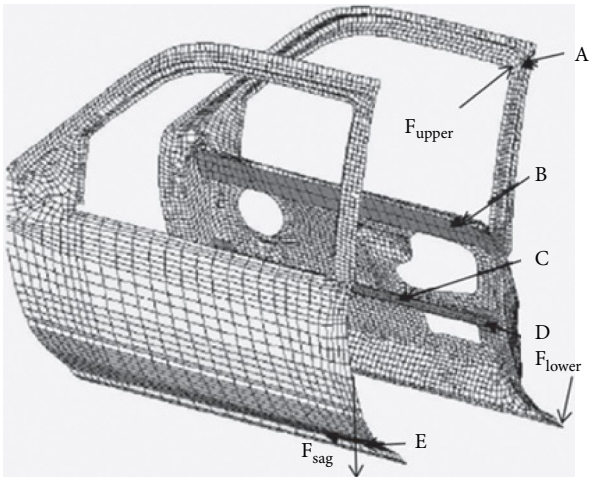

Figure 3: Finite element analysis of door structure.

due to the constraints of the upper and lower degrees of freedom of the door. On this basis, the concentrated load in the horizontal direction appears on the upper and lower parts of the door, and the average value is expressed as 200 N. The deformation of the load concentration point of the door is used as its stiffness measurement index, and then the door model is established and the finite element analysis of the stress load is carried out.

The analysis process is a static analysis, load is applied to it, the load application positions are set at 150 mm and 300 mm, respectively, and the load application time is set at 0.01 s and 0.15s, respectively. The simulation found that the deformation of the door was small when the load application position was 150 mm (0.01 s) during the load application process. At this time, the load was transferred to the outer door panel, and the outer panel appeared bending phenomenon after the load was applied. Under this load, the door itself cannot provide the endurance to cope with the load. When the load application position is set to 300 mm (0.15 s), the structure is completely unable to cope with its load. At this time, the door is subjected to a large load, which causes the structure to be damaged, and squeezes the inner plate structure of the rear door structure, which is an energy-absorbing element, and the anticollision beam of the door structure itself also consumes more energy after being loaded, and the energy absorbed by the door reinforcing plate structure is less.

According to the load characteristics of the above structural model, the optimized model analysis of the structure can be carried out, and its reinforcing plate, anticollision beam frame, bracket, inner plate, and outer plate are set as five variables in the model design, which are, respectively, expressed as $T = \{t_1, t_2, t_3, t_4, t_5\}$T; on this basis, the quality of the door can be taken as the optimization target of this model. In view of the research content of this paper, the door should be able to withstand a certain range of loads in different regions under the action of static load. Combined with multiple criteria, the final research standard in this paper is that the initial endurance of the door should be ≥ 10 N, and the endurance of the door in the intermediate stage should be ≥ 15 N, and the pressure on the door during the whole loading process must be ≥ 35 N.

Table 1: Uniform design table.

Num	t_2	t_3	t_4	t_5
1	1	4	5	5
2	2	3	4	2
3	3	7	6	11
4	4	1	7	12
5	5	2	1	3
6	6	7	12	4
7	7	4	2	1
8	8	9	3	6
9	9	10	11	9
10	10	12	9	7
11	11	6	10	8
12	12	8	8	10

The door stiffener structure absorbs less energy during periods when the door is under load, thus eliminating the associated variables set forth above. Then, set its anticollision beam frame, bracket, inner plate, and outer plate as several variables of model design, and express them as $T = \{t_2, t_3, t_4, t_5\}^T$, respectively. In this paper, 12 factor levels are set for the above four factors in combination with the orthogonal test. Combined with the initial pressure resistance and intermediate pressure resistance expression formula obtained in the previous section, the uniform design table of quasi-static extrusion response can be obtained, as shown in Table 1.

Combined with the optimization model in the above file and the parameter design of each part, the parameters of the door components are optimized through the optimization algorithm, and the model optimization results are obtained. The optimization results shown in Table 2 and 3 are obtained.

Based on the optimization of the multi-material combination of the door of the most important part of the body, the lightweight design of the body can be carried out. In this paper, other parts are comprehensively analyzed and orthogonal tests are carried out to obtain the degree of importance of influencing factors on vehicle quality. In order to further reduce the mass of the car body, it is necessary to establish the objective function with the mass as the optimization objective. The structure is lightweight through the effective cooperation of multiple materials, and the cost is taken as a basic reference factor in the actual design.

On the basis of the multi-material vehicle model established above, a related optimization model is established combined with the multi-material vehicle designed in this paper. In the actual design, the goal of the function model is to minimize the body mass, and to ensure the lowest cost, so that it can be applied in practice in automobile production. There are mainly 13 factors that affect the quality of the car body, and the factors with higher influence can be selected as the optimization direction. This study adopts a multi-material optimization strategy for vehicle body optimization. Moreover, this paper sets several candidate materials for each beam structure component of

Table 2: Results of structural optimization parameters.

	Reinforcing plate (mm)	Crash beam frame (mm)	Bracket (mm)	Inner plate (mm)	Outer panel (mm)	Structural quality (kg)	Structure fee ($)
Low-carbon steel	0.66	2.53	2.33	1.08	1.30	19.01	13.33
High strength steel	0.66	1.97	1.08	1,01	0.96	15.34	14.23
Aluminum alloy	1.06	1.03	2.45	2.00	1.57	10.31	23.12
Magnesium alloy	1.06	1.03	1,17	2.97	1.46	8.56	24,67

Table 3: Performance after structural optimization.

Material	F_{sag} (mm)	F_{upper} (mm)	F_{lower} (mm)	w (Hz)
Low-carbon steel	1.46	1.91	0.87	38
High strength steel	1.96	2.47	1.82	36
Aluminum alloy	1.56	2.57	1.46	41
Magnesium alloy	1.36	2.57	1.33	54

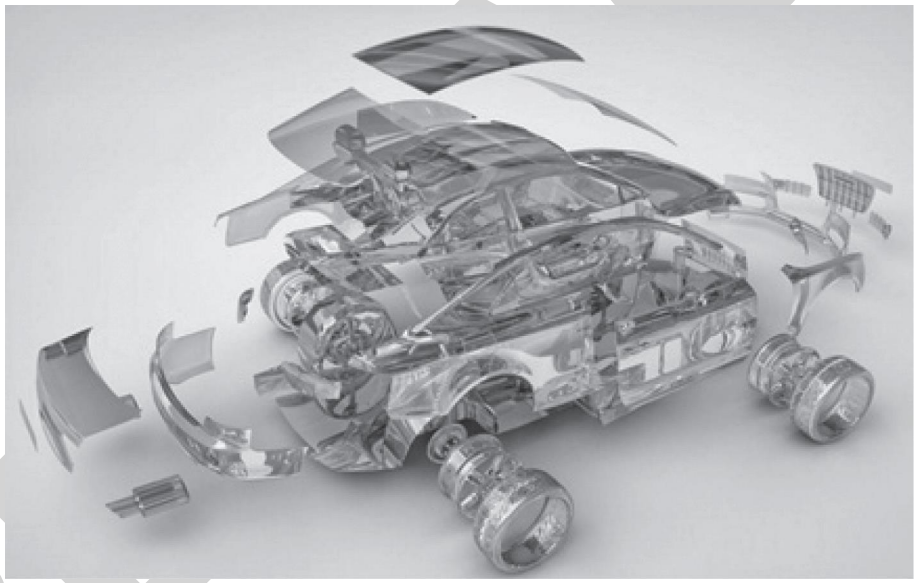

Figure 4: Split diagram of auto parts.

the car and uses low carbon steel as a single car body material for comparison and uses magnesium alloy, aluminum alloy, and carbon fiber as the alternative materials. In addition, we numbered magnesium alloy, aluminum alloy, low carbon steel, and carbon fiber as 1#, 2#, 3#, and 4# and combined the previous model building methods to build the above materials as variables to build a multi-material vehicle body quality optimization model. Figure 4 is the split diagram of auto parts.

After model processing, multiple parts of the car are comprehensively optimized, and the multi-material structure optimization design combination solution is obtained, which is compared with the single-material body. The comparison finds that corresponding solutions can be obtained for different situations, and on this basis, the results obtained are analyzed. By comparing the results, it can be seen that a certain solution set cannot be regarded as the optimal solution, and different solutions corresponding to different needs are feasible. Therefore, when carrying out the lightweight design of the body, the combination optimization results that can be effectively combined should be selected according to the user's needs and use occasions, as shown in Table 4.

It can be seen from Table 5 that the proportion of lightweight materials in the multi-material continues to increase in the process of vehicle body optimization. For example, the use of all-aluminum body will reduce the weight of the car body by 16.53%, and the corresponding cost will increase by 111.99%. Based on this, the all-aluminum body can be applied to some luxury car

Table 4: Multi-material combination of automobile body.

Serial number	Multi-material combination
a	Low-carbon steel 70% + aluminum alloy 20% + magnesium alloy 10%
b	Low-carbon steel 50% + aluminum alloy 30% + magnesium alloy 20%
c	Low-carbon steel 40% + aluminum alloy 30% + magnesium alloy 30%
d	Low-carbon steel 30% + aluminum alloy 40% + magnesium alloy 30%
e	Low-carbon steel 20% + aluminum alloy 30% + magnesium alloy 20% + carbon fiber 30%
f	Low-carbon steel 20% + aluminum alloy 20% + magnesium alloy 20% + carbon fiber 40%

Table 5: Optimization results of lightweight design combination of multi-material structure vehicles.

Serial number	Weight (kg)	Cost ($)	Percent weight loss (%)	Cost increase ratio (%)	Cost-to-quality ratio ($/kg)
Low-carbon steel	85.34	60.12	0.00	0.00	0.00
a	80.87	71.34	5.24	18.66	2.51
b	78.45	74.32	8.07	23.62	2.06
Aluminum alloy	71.23	127.45	16.53	111.99	4.77
c	66.54	134.09	22.03	123.04	3.93
d	64.21	171.78	24.76	185.73	5.28
e	61.17	211.98	28.32	252.59	6.28
f	51.23	443.97	39.97	638.47	11.25

manufacturing. If the cost of automobile manufacturing is not considered in automobile manufacturing, carbon fiber can be used to the maximum extent as the body material to achieve the greatest weight reduction effect.

From the above research, it is verified that computer-aided technology can play an important role in vehicle structure optimization and effectively improve the scientificity of vehicle structure design.

4. Conclusion

The purpose of structural optimization design is to solve the contradiction between the structural static and dynamic performance such as structural deformation, stiffness, stress, strength, and fundamental frequency and the available design resources such as structural weight (mass), cost, and volume. It designs the structure with the best performance with the least design resources, so as to improve the product cost performance and product market competitiveness as much as possible. The essence of structural optimization design is to allocate design resources reasonably, so that design resources such as quality are allocated reasonably within the geometrical space of the structure and among the components. The main feature of structural optimization design is that the static and dynamic properties of the structure (displacement and stress, etc.) and the static and dynamic characteristics of the structure (resonant frequency, etc.), which are the objective function and the constraint function, are generally high-order nonlinear implicit functions of the structural design variables. It can be obtained by modern numerical analysis methods such as finite element analysis. In addition, this paper combines the computer-aided technology to carry out the vehicle structure optimization design, and the research verifies that the computer-aided technology can play an important role in the vehicle structure optimization and effectively improve the scientificity of the vehicle structure design.

Data Availability

The labeled dataset used to support the findings of this study is available from the author upon request.

Conflicts of Interest

The author declares no conflicts of interest.

Acknowledgments

This work was supported by Jilin Baicheng Normal University.

References

[1] X. Sun, J. Liu, B. Lu, P. Zhang, and M. Zhao, "Life cycle assessment-based selection of a sustainable lightweight automotive engine hood design," *International Journal of Life Cycle Assessment*, vol. 22, no. 9, pp. 1373–1383, 2017.

[2] G. Mostyn, "Meeting advanced automotive design challenges with mems-based timing devices," *Electronics World*, vol. 124, pp. 20–23, 2018.

[3] J. Iván, "High power printed circuit board design for automotive fuse block usage," *Dyna*, vol. 84, no. 203, pp. 88–94, 2017.

[4] J. Alfonso-Beltrán, I. J. Bautista, and C. Barrios, "Occupational risk factors for shoulder chronic tendinous pathology in the Spanish automotive manufacturing sector: a case-control study," *BMC Musculoskeletal Disorders*, vol. 21, no. 1, pp. 818–8, 2020.

[5] P. Polverino, E. Frisk, D. Jung, M. Krysander, and C. Pianese, "Model-based diagnosis through structural analysis and causal computation for automotive polymer electrolyte membrane fuel cell systems," *Journal of Power Sources*, vol. 357, no. Jul.31, pp. 26–40, 2017.

[6] X. Wei, H. Yuan, H. Wang, and Y. Chen, "Intelligent design for automotive interior trim structures based on knowledge rule-based reasoning," *International Journal of Automotive Technology*, vol. 21, no. 5, pp. 1149–1167, 2020.

[7] R. A. Poshekhonov, G. A. Arutyunyan, S. A. Pankratov, A. S. Osipkov, D. O. Onishchenko, and A. I. Leontyev, "Development of a mathematical model for optimizing the design of an automotive thermoelectric generator taking into account the influence of its hydraulic resistance on the engine power," *Semiconductors*, vol. 51, no. 8, pp. 981–985, 2017.

[8] F. Uysal, "Phase-coded fmcw automotive radar: system design and interference mitigation," *IEEE Transactions on Vehicular Technology*, vol. 69, no. 1, pp. 270–281, 2020.

[9] N. Geren, O. O. Akçalı, and M. Bayramoğlu, "Parametric design of automotive ball joint based on variable design methodology using knowledge and feature-based computer assisted 3d modelling," *Engineering Applications of Artificial Intelligence*, vol. 66, no. nov, pp. 87–103, 2017.

[10] M. Mcharek, T. Azib, M. Hammadi, C. Larouci, and J.-Y. Choley, "Multiphysical design approach for automotive electronic throttle body," *IEEE Transactions on Industrial Electronics*, vol. 67, no. 8, pp. 6752–6761, 2020.

[11] Y. Xie, G. Zeng, R. Kurachi, X. Peng, G. Xie, and H. Takada, "Balancing bandwidth utilization and interrupts: two heuristic algorithms for the optimized design of automotive cps," *IEEE Transactions on Industrial Informatics*, vol. 16, no. 4, pp. 2382–2392, 2020.

[12] J. P. Trovao, "Digital transformation, systemic design, and automotive electronics [automotive electronics]," *IEEE Vehicular Technology Magazine*, vol. 15, no. 2, pp. 149–159, 2020.

[13] H. C. Kim, T. J. Wallington, and J. L. G. A. Sullivan, "Commentary on "Correction to: on the calculation of fuel savings through lightweight design in automotive life cycle assessments" by Koffler and Rohde-Brandeburger (2018)," *International Journal of Life Cycle Assessment*, vol. 24, no. 3, pp. 397–399, 2019.

[14] E. Di Pasquale and D. Coutellier, "Wave propagation in head on bonnet impact: material and design issues," *International Journal of Automotive Technology*, vol. 18, no. 4, pp. 631–642, 2017.

[15] A. Nordelöf, E. Grunditz, A.-M. Tillman, T. Thiringer, and M. Alatalo, "A scalable life cycle inventory of an electrical automotive traction machine-Part I: design and composition," *International Journal of Life Cycle Assessment*, vol. 23, no. 1, pp. 55–69, 2018.

[16] H. S. Ayoub, W. M. Hussein, A. F. El-Sherif, and Y. H. Elbashar, "Design and test of high-efficiency dual-element laser diffuser for large-field automotive shadowgraphy," *Journal of Optics*, vol. 49, no. 2, pp. 263–269, 2020.

[17] S. Kongwat, P. Jongpradist, and H. Hasegawa, "Lightweight bus body design and optimization for rollover crashworthiness," *International Journal of Automotive Technology*, vol. 21, no. 4, pp. 981–991, 2020.

[18] N. S. B. Yusof, S. M. Sapuan, M. T. H. Sultan, and M. Jawaid, "Conceptual design of oil palm fibre reinforced polymer hybrid composite automotive crash box using integrated approach," *Journal of Central South University*, vol. 27, no. 1, pp. 64–75, 2020.

[19] S. M. Hosseini, M. Arjomandi Rad, A. Khalkhali, and M. J. Saranjam, "Optimal design of the s-rail family for an automotive platform with novel modifications on the product-family optimization process," *Thin-Walled Structures*, vol. 138, no. MAY, pp. 143–154, 2019.

[20] T. J. Wang and S. K. Hwang, "Combustion system design of a genset diesel engine by using dfss methodology," *International Journal of Automotive Technology*, vol. 20, no. 3, pp. 539–547, 2019.

[21] G. Xie, H. Peng, J. Huang, R. Li, and K. Li, "Energy-efficient functional safety design methodology using ASIL decomposition for automotive cyber-physical systems," *IEEE Transactions on Reliability*, vol. 68, pp. 1–23, 2019.

[22] D. J. Belgiovane, C.-C. Chen, S. Y. P. Chien, and R. Sherony, "Surrogate bicycle design for millimeter-wave automotive radar pre-collision testing," *IEEE Transactions on Intelligent Transportation Systems*, vol. 18, pp. 2413–2422, 2017.